OpenFOAM hybrid - A Morphology Adaptive Multifield Two-fluid Model

Schlegel, F.; Meller, R.; Krull, B.; Lehnigk, R.; Tekavcic, M.;

Originally published:

November 2022

Nuclear Science and Engineering 197(2022)10, 2620-2633

DOI: https://doi.org/10.1080/00295639.2022.2120316

OpenFOAM-Hybrid – A Morphology Adaptive Multifield Two-Fluid Model

Fabian Schlegel,[*,a] Richard Meller,[a] Benjamin Krull,[a] Ronald Lehnigk,[a] and Matej Tekavčič[b]

[a] *Helmholtz-Zentrum Dresden - Rossendorf, Institute of Fluid Dynamics, Bautzner Landstr. 400, 01328 Dresden, Germany*

[b] *Jožef Stefan Institute, Reactor Engineering Division Jamova cesta 39, 1000 Ljubljana, Slovenia*

[*]Email: f.schlegel@hzdr.de

Number of pages: 25
Number of tables: 2
Number of figures: 10

Abstract

Industrial multiphase flows are typically characterized by coexisting morphologies. Modern simulation methods are well established for dispersed (e.g., Euler-Euler) or resolved (e.g., Volume-of-Fluid) interfacial structures. Hence, a morphology adaptive multifield two-fluid model is proposed, which is able to handle dispersed and resolved interfacial structures coexisting in the computational domain with the same set of equations. The interfacial drag formulation of Štrubelj and Tiselj (Int J Numer Methods Eng, 2011, Vol. 85, 575-590) is used to describe large interfacial structures in a volume-of-fluid-like manner. For the dispersed structures, the baseline model developed at Helmholtz-Zentrum Dresden – Rossendorf is applied. The functionality of the framework is demonstrated by investigating a single rising gas bubble in a stagnant water column, a 2D stagnant stratification of water and oil, sharing a large-scale interface, which is penetrated by micro gas bubbles, and an isothermal counter-current stratified flow case. Recent developments focus on the transition region, where bubbles are over- or under-resolved either for Euler-Euler or for Volume-of-Fluid. Furthermore, a concept is presented for the transition of oversized dispersed bubbles into the resolved phase.

Keywords — Multiphase Flows, Numerical Simulation, Hybrid Model, OpenFOAM, Euler-Euler

I. INTRODUCTION

Multiphase flows are characterized by a very high level of complexity. Especially in industrial applications, various different flow regimes can appear even in very simple geometries. A common example are pipe flows, where segregated, bubbly, annular or slug flows can occur. The level of complexity increases, if, e.g. countercurrent flows or wave breaking phenomena are of interest. Furthermore, different morphologies often occur simultaneously, like large-scale interfaces (a boundary between two immiscible phases) together with dispersed structures (small bubbles or droplets), or even dispersed structures of different sizes and shape that interact with each other and might form a large-scale interface downstream. Examples with relevance for industrial applications are an impinging jet with bubble entrainment that occurs for instance during pressurized thermodynamic shock scenarios (PTS, [1]), centrifugal pumps, swirling flow separators, fractionating columns, etc. For each main flow morphology, suitable modeling approaches exists, which are usually characterized by different levels of complexity and computational efficiency. On the one hand, for interfaces that are large enough to be resolved on a given grid, Lagrangian methods are available, namely marker and cell or front-tracking methods. Furthermore, Eulerian methods have been developed for the same purpose, such as level-set, conservative level-set or volume-of-fluid (VOF, with geometric or algebraic interface reconstruction) methods. On the other hand, for interfaces that are too small to be resolved on the grid (so called dispersed phases), Euler-Lagrange and Euler-Euler methods have proven their applicability and reliability for various applications.

However, for many complex applications the information about the flow morphology is not known a priori. Hence, a simulation method that requires less knowledge about the flow in advance would be desirable and should allow describing both interfacial structures – resolved and dispersed – in a single computational domain. Such methods that combine interface-resolving and non-resolving approaches are called *hybrid model*s. Several attempts to develop such a model have been made so far. Herrmann [2] and Ma et al. [3] combined Lagrangian point particle methods with a level-set method, whereas Hua [4] combined the first with a VOF method. Numerous publications are available which refer to the blending of Euler-Euler with VOF or VOF-like models, e.g. Boualouache et al. [5], Yan and Che [6], Černe et al. [7], Lopes et al. [8], Hundshagen et al. [9, 10], De Santis et al. [11] and Colombo et al. [12]. For nuclear safety analysis, special attention has been paid to stratified flows modeling unresolved interface features, e.g. by Coste et al. [13],

Porombka and Höhne [14], Rezende et al. [15], and Höhne and Porombka [16]. Following the same idea, but not limited to stratified flows, Wardle and Weller [17], Shonibare and Wardle [18] and Mathur et al. [19] presented a VOF-like approach without interface reconstruction that was combined with Euler-Euler modeling for dispersed flows, but strictly limited to two fields. A suitable blending method based on the phase fraction ensures that the two-fluid model behaves either as a VOF-like model or as a dispersed Euler-Euler model. This firstly requires the formulation of the interfacial momentum exchange terms for all possible regimes, most importantly the drag term, and, secondly, the extension of the two-fluid model formulation by an interface-tracking method. For the latter, Wardle and Weller [17] used an artificial interface compression term in the transport equation for the phase fractions developed by Weller [20] to suppress numerical diffusion near resolved interfaces. For the momentum exchange for the resolved interfaces, they used a residual drag formulation that allowed for a residual slip velocity. The main limitations of this approach are that interactions between multiple dispersed phases or between a dispersed phase and two different continuous phases cannot be covered, and that the numerical error of the method might influence the morphology transitions. Furthermore, the definition of the residual slip velocity is somewhat arbitrary and has to be adjusted for every simulation.

As a logical consequence in the present work, dispersed and continuous phases have to be simulated as individual numerical phases and phase transfer models have to be established to describe the transitions between them. Such an approach was proposed by Hänsch et al. [21] and, recently, has been adopted by Frederix et al. [22]. In the following, the theory of a numerical framework is presented, which incorporates a multifield two-fluid model that is able to account for resolved interfaces and the transition between resolved and dispersed morphologies. The term two-fluid model refers to the idea of interpenetrating continua and does not necessarily imply that the model is restricted to two numerical phases. Furthermore, simple applications are shown, which demonstrate the predictive capabilities of the framework before an advanced outlook on the currently ongoing developments is given.

II. MORPHOLOGY ADAPTIVE MULTIPHASE TWO-FLUID MODEL

The following section is a comprehensive review of Meller et al. [23] and Tekavčič et al. [24] and introduces briefly the theory and the numerical basis of the proposed morphology adaptive

multifield two-fluid model, from now on named *hybrid model*. More details about the implementation can be found in the aforementioned publications. The main design criteria for the presented *hybrid model* are:

- In the long term, the model is supposed to be used for industrial applications in the fields of nuclear safety analysis and chemical and process engineering. Hence, compromises in favor of computational efficiency that might affect accuracy are acceptable to a certain extent.
- Phases representing dispersed and continuous morphologies should be treated with the same, generalized set of equations, i.e. no blending between morphologies.
- In the limits of sufficiently resolved large interfaces or sufficiently under-resolved dispersed interfaces, the *hybrid model* has to recover an algebraic VOF or the well-known Euler-Euler model, respectively (edge cases for the *hybrid model*).
- Continuous and dispersed phases are represented by individual numerical phases to allow the highest amount of flexibility and to avoid numerically driven morphology changes.
- Suitable mass transfer models need to be accounted for the transition between morphologies, namely dispersed to resolved and vice versa.
- Dispersed phases should be able to interact with or cross a resolved interface.

Hence, the framework for the *hybrid model* consists of

1. multiple phase-specific, ensemble-averaged transport equations for individual continuous and dispersed phases,
2. a set of closure models for the interfacial momentum transfer terms for dispersed flows,
3. an induced turbulence framework for dispersed flows,
4. a class method to model the size distribution of the dispersed structures by means of a population balance equations together with suitable models for breakup and coalescence [25],
5. an interfacial drag formulation to represent large scale, resolved interfaces in the two-fluid model with the interface compression term of Weller [20], and

6. a turbulence dampening strategy to dampen turbulence in the vicinity of resolved interfaces [24].

As the two-fluid model forms the basis of the presented framework, the ensemble averaged mass and momentum conservation equations for each phase α read

$$\partial_t r_\alpha \rho_\alpha + \partial_i r_\alpha \rho_\alpha u_{\alpha,i} = 0 \tag{1}$$

$$\partial_t r_\alpha \rho_\alpha u_{\alpha,i} + \partial_j r_\alpha \rho_\alpha u_{\alpha,i} u_{\alpha,j} = -r_\alpha \partial_i p + \partial_j 2 r_\alpha \mu_\alpha S_{\alpha,ij} + r_\alpha g_i \rho_\alpha + \sum_{\beta \neq \alpha} r_\alpha \sigma_{\alpha\beta} \kappa_{\alpha\beta} n_{\alpha\beta,i} + f_{\alpha,i}, \tag{2}$$

where r_α represents the phase fraction of phase α, ρ_α its phase-specific density, u_α the velocity vector of the phase, p the pressure shared between all phases, μ_α the dynamic viscosity, S_α the strain rate tensor, $\vec{g}$ the gravitational acceleration with a value of $9.81\,\mathrm{ms}^{-1}$, $\sigma_{\alpha\beta}$ the surface tension between phase pair α and β, $\kappa_{\alpha\beta}$ the interface curvature, $\vec{n}_{\alpha\beta}$ the interface normal vector, and $\vec{f}_\alpha$ the interfacial momentum exchange terms. For bubbly flows, the latter terms consist of closure models for drag, lift, virtual mass, wall lubrication and turbulent dispersion. Furthermore, a turbulence model with an additional bubble induced turbulence term is required for the continuous phase. Those closure models are selected according to the baseline model developed at Helmholtz-Zentrum Dresden – Rossendorf (HZDR). As the focus of the present work is the *hybrid model*, and for sake of clarity, the reader is referred to the work of Rzehak and Krepper [26], Liao et al. [27] and Hänsch et al. [28] for details about the baseline model development and the most up-to-date correlations.

A key feature of the presented *hybrid model* is the incorporation of resolved interfaces within the two-fluid model. One of the reasons for choosing the two-fluid model is that it provides a large degree of freedom – which is a challenge on the one hand, but gives more opportunities on the other hand, in particular for the transition region as shown later. A necessary condition for a resolved interface is that the local velocity components normal to an interface formed by two continuous phases have to be identical. However, the demand of recovering an algebraic VOF method as an edge case for sufficiently resolved interfaces imposes a much stronger no-slip condition to the interface. It was shown by Yan and Che [6] that the two-fluid model collapses into the homogeneous (VOF) model, in case the interface velocities are identical. A suitable drag model was proposed

by Štrubelj and Tiselj [29], which reads

$$f^D_{\alpha\beta,i} = r_\alpha r_\beta \rho_{\alpha\beta} \frac{1}{\tau_r}(u_{\beta,i} - u_{\alpha,i}), \tag{3}$$

with the mixture density

$$\rho_{\alpha\beta} = \frac{\rho_\alpha r_\alpha + \rho_\beta r_\beta}{r_\alpha + r_\beta}. \tag{4}$$

and τ_r as the relaxation time that has to be chosen much smaller than the physical time step.

Another important aspect requiring attention is the over-prediction of the turbulent kinetic energy near large interfaces. This is particularly important for stratified flow cases, but has to be investigated for large, resolved bubbles in future. Hence, a turbulence damping method based on the model originally proposed by Egorov [30] is added to the *hybrid model*. The idea of this model is to mimic a wall-like damping of turbulence near an interface, as reported by Fulgosi et al. [31]. The turbulence damping term is added to the ω-transport equation of the k-ω SST turbulence model proposed by Menter et al. [32]

$$\begin{aligned} &\partial_t r_\alpha \rho_\alpha \omega_\alpha + \partial_i r_\alpha \rho_\alpha u_{\alpha,i} \omega_\alpha \\ &= \partial_i r_\alpha \left(\mu_\alpha + \sigma_\omega \mu^T_\alpha\right) \partial_i \omega_\alpha + \frac{r_\alpha \rho_\alpha \gamma}{\mu^T_\alpha} \widetilde{P_\alpha} - \beta r_\alpha \rho_\alpha \omega^2_\alpha + 2(1 - F_1) \frac{r_\alpha \rho_\alpha \sigma_{\omega 2}}{\omega_k} \partial_i k_\alpha \partial_i \omega_\alpha + S^\omega_\alpha, \end{aligned} \tag{5}$$

where ω_α is the specific turbulent dissipation rate, μ_α and μ^T_α are the dynamic molecular viscosity and the eddy viscosity, respectively, and k_α the turbulent kinetic energy of phase α. The remaining coefficients, namely β, σ_ω, $\sigma_{\omega,2}$, γ and F_1, are model constants of the k-ω SST turbulence model and $\widetilde{P_\alpha}$ represents the production term for the turbulent kinetic energy. The turbulence damping term S^ω_α counteracts the destruction term $-\beta r_\alpha \rho_\alpha \omega^2_\alpha$ for the specific turbulent dissipation rate and is defined according to the expression used by Frederix et al. [33]

$$S^\omega_\alpha = A r_\alpha \beta \rho_\alpha \left(\frac{\mu_\alpha}{\rho_\alpha \beta \delta^2_\alpha}\right)^2 \tag{6}$$

with the damping length scale δ_α and A as the interface indicator field, which is only non-zero at the interface.

The presented hybrid approach is implemented in the open source library OpenFOAM, a state-of-the-art library dedicated to numerical simulations of fluid dynamic problems. The full

TABLE I
Overview over gravitational scales and dimensionless numbers of cases of rising gas bubble (G) in liquid (L) of Balcázar et al. [38].

Case	Re_g	$\mathrm{Re}_b^{\mathrm{Bal}}$	Eo	Mo	$\frac{\rho_L}{\rho_G}$	$\frac{\mu_L}{\mu_G}$	U_g	t_g
1	11	6.94	116	41.1	100	100	$3.132\,\mathrm{ms}^{-1}$	0.319 s
2	31	17.46	339	43.1	100	100	$3.132\,\mathrm{ms}^{-1}$	0.319 s

source code of the presented *hybrid model* is available open source following the FAIR principles (Findability, Accessibility, Interoperability, and Reuse of digital assets, [34]). OpenFOAM features a finite volume method and the partial differential equations are solved numerically on a collocated grid in a segregated manner. The drag model according to Štrubelj and Tiselj [29] results in a stiff equation system, which requires the implementation of an n-phase partial elimination algorithm [23]. Furthermore, the compact momentum interpolation for multiphase flows according to Cubero et al. [35] is utilized to ensure consistency in terms of time step, relaxation factor and drag force. The pressure velocity coupling is resolved by means of a projection method. The discretization is second order accurate in space and first order implicit in time. The phase fraction equations are explicitly integrated in time with a multidimensional limiter for an explicit solution algorithm (MULES, [36]) and a flux-limiting scheme for the convection term by van Leer [37]. Finally, the interface compression scheme of Weller [20] is applied to prevent resolved interfaces from diffusing due to numerical diffusivity.

III. APPLICATION OF THE HYBRID MODEL TO VARIOUS SCENARIOS

The following section briefly introduces three simulation cases, which are supposed to demonstrate the capabilities of the presented *hybrid model* and serve as basic verification tests. The focus is on resolved interfaces, as this is the main challenge that has to be solved. More details on the simulation setups can be found in Meller et al. [23] and in Tekavčič et al. [24].

III.A. Three-dimensional Rising Bubble

This test case is a classical scenario for VOF methods. The idea is to demonstrate the capability of the *hybrid model* to simulate a single rising bubble in a stagnant water column with similar results as a comparable algebraic VOF. The setup follows Balcázar et al. [38] and the dimensionless parameters for the selected cases are listed in Table I. The bubble is initialized as a

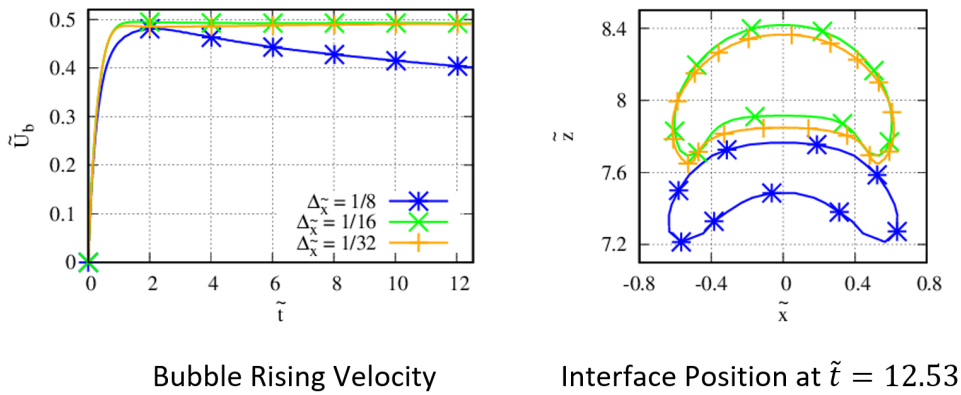

Fig. 1. Bubble rising velocity and interface position ($r_\alpha = 0.5$) at $\tilde{t} = 12.53$ for different spatial resolutions in three-dimensional rising bubble case 1.

sphere with a diameter D_b at the horizontal center of the computational domain, $2\,D_b$ above the bottom. The computational domain is a cylindrical vessel with a diameter of $8\,D_b$ and a height of $12\,D_b$. The bubble diameter is used to define any dimensionless length as

$$\widetilde{L} = \frac{L}{D_b}. \tag{7}$$

Furthermore, gravitational velocity $U_g = \sqrt{gD_b}$, gravitational time scale $t_g = \sqrt{D_b/g}$, dimensionless velocity $\widetilde{U} = U/U_g$ and dimensionless time scale $\widetilde{t} = t/t_g$ are defined. The dimensionless numbers Reynolds number, Eötvös number and Morton number are defined as $\mathrm{Re}_g = \rho_L U_g D_b/\mu_L$, $\mathrm{Eo} = \rho_L g D_b^2/\sigma$ and $\mathrm{Mo} = g\mu_L^4(\rho_L - \rho_G)/(\rho_L^2\sigma^3)$, respectively. The indices G and L represent gas and liquid properties, respectively. An orthogonal equidistant grid is used in the center of the domain. Towards the shell surface of the cylinder the grid is radially stretched with the aim to reduce computational costs. The mesh spacing was selected based on a grid study, where some exemplary results are shown in Fig. 1. For the results presented in the following the grid spacing is fixed to $\Delta_{\widetilde{x}} = 1/32$. The boundary conditions are free-slip for the lateral walls of the cylindrical domain, no-slip at the bottom wall and a free gas-liquid surface is established $1\,D_b$ below the upper boundary. The pressure is fixed at the top boundary. A sketch of the domain, the grid used and the initial position of the bubble and the free surface is given in Fig. 2.

The results of the present solver are compared to the results obtained by Balcázar et al. [38] and the results of *interFoam*, which is the default solver in OpenFOAM that implements an algebraic VOF. As known for algebraic VOF the time step plays an important role and, hence, is

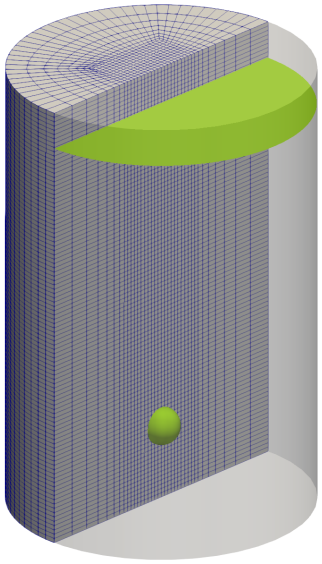

Fig. 2. Computational domain (gray) and grid (blue) as well as initial interface position (green) of three-dimensional rising bubble cases.

fixed to $\Delta_{\widetilde{t}} = 3.13 \cdot 10^{-2}$, which results in a Courant number of less than 0.12. Figure 3 shows dimensionless bubble rising velocity $\widetilde{U}_b$ and the sphericity s_b over time as well as interface location $r_G = 0.5$ at dimensionless time $\widetilde{t} = 12.53$ for case 1 (see Table I). The bubble sphericity s_b is defined as the ratio of the surface area of a sphere with equivalent volume to the actual bubble surface area.

It is evident from Fig. 3(b) that at the beginning of the simulation, for $\widetilde{t} < 4$, the bubble rising velocity predicted with the present solver is slightly smaller than the one obtained with *interFoam*. Nevertheless, in the second half of the simulation, both values approach each other. Compared to the level-set results of Balcázar et al. [38], both OpenFOAM solvers predict a slightly lower value. In terms of bubble shape, both solvers perform very similar in the beginning of the simulation, whereas the *hybrid model* predicts slightly lower values towards the end of the simulations. However, the comparison of the bubble shape between Balcázar et al. [38], *interFoam* and the present solver at $\widetilde{t} = 12.53$ shows a very good agreement. Apart from the skirt region, which is characterized by a high interface curvature, nearly no differences in bubble shape can be observed.

For case 2, the results are shown in Fig. 4 in terms of the same quantities as for case 1. Both solvers, *interFoam* and the present solver, predict a deceleration of the bubble in the second half

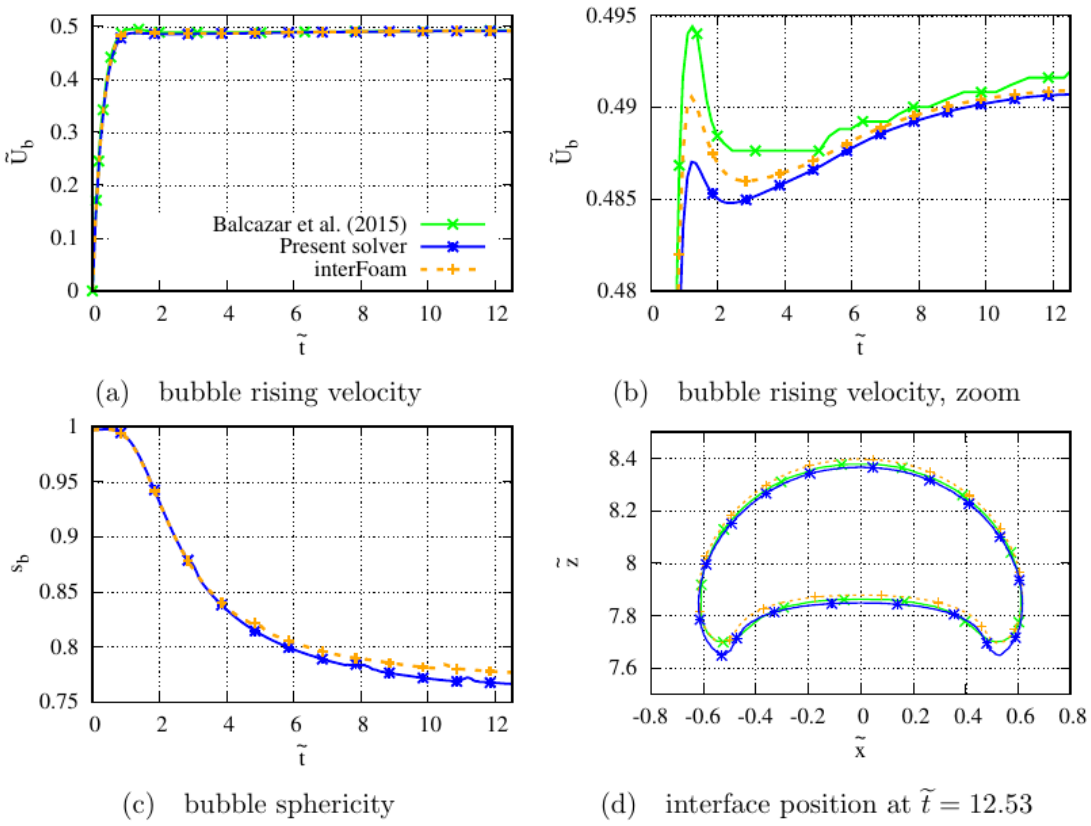

(a) bubble rising velocity (b) bubble rising velocity, zoom

(c) bubble sphericity (d) interface position at $\tilde{t} = 12.53$

Fig. 3. Bubble rising velocity and sphericity over time as well as interface position ($r_G = 0.5$) at $\tilde{t} = 12.53$ for three-dimensional rising bubble case 1. Data for interface position of Balcázar et al. [38] are adjusted in terms of scale and position.

of the simulation. Due to this, an under-prediction of 3 % in rising velocity is observed compared to Balcázar et al. [38]. However, when looking at the bubble shape at $\tilde{t} = 12.53$ both OpenFOAM solvers show the same results, differing slightly from the results of Balcázar et al. [38]. The ligaments predicted by Balcázar et al. [38] are slightly shorter and the gas-liquid interface between them is flat. However, in summary the present solver shows nearly identical results to a default algebraic VOF method implemented in interFoam. Some moderate differences to the more accurate level-set method have been found, but overall the agreement is satisfying.

III.B. Two-Dimensional Stagnant Stratification of Water and Oil with Air Bubbles

An important design criterion already mentioned is the capability of the framework to handle interactions of dispersed phases with an interface between two other continuous phases. For testing purposes, a bubble column with a width of 0.15 m and a height of 0.5 m was defined. Dispersed air bubbles with a diameter of $D_{\text{air}} = 1\,\text{mm}$ are introduced into a stagnant stratification of oil and water (50% of the domain filled with each phase). The grid is equidistant with a grid spacing

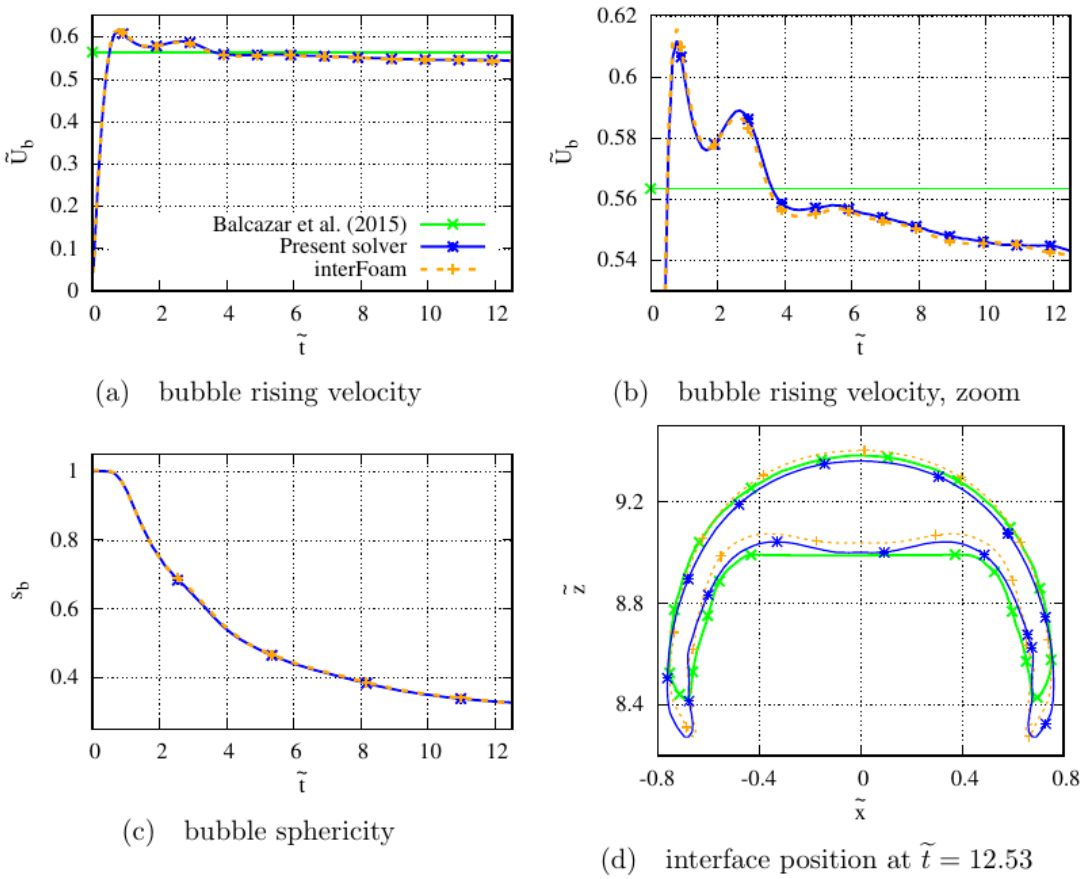

(a) bubble rising velocity

(b) bubble rising velocity, zoom

(c) bubble sphericity

(d) interface position at $\tilde{t} = 12.53$

Fig. 4. Bubble rising velocity and sphericity over time as well as interface position ($r_G = 0.5$) at $\tilde{t} = 12.53$ for three-dimensional rising bubble case 2. Data for interface position of Balcázar et al. [38] are adjusted in terms of scale and position.

of $\Delta_x = \Delta_y = 0.005\,\mathrm{m}$. The top boundary is a fixed-pressure boundary condition, whereas at the lateral boundaries a no-slip condition for water and oil and a free-slip condition for the gas is imposed. The dispersed gas is injected at the bottom of the domain in a region between $0.05\,\mathrm{m} < x < 0.1\,\mathrm{m}$ with a void fraction of $r_{\mathrm{air}} = 0.26$ and a wall-normal velocity of $U_{\mathrm{air}} = 0.197\,\mathrm{ms}^{-1}$. The time step is set to $\Delta_t = 0.03\,\mathrm{s}$. The closure models for phase pairs formed by a continuous and a dispersed phase are defined according to Ishii and Zuber [39] for drag and Crowe et al. [40] for virtual mass ($C_{\mathrm{VM}} = 0.5$). The drag model for a pair of continuous phases is the aforementioned model of Štrubelj and Tiselj [29]. The material properties of the phases are listed in Table II.

The time resolved results in Fig. 5 show how the swarm of bubbles enters the domain and forms a mushroom shaped cloud afterwards. At $t \approx 1.6\,\mathrm{s}$, the swarm hits the water-oil interface, penetrates it and continues rising towards the top boundary. The water-oil interface temporarily deforms when the bubble swarm passes, keeps sloshing for a while, and, finally, almost perfectly recaptures at its initial position. The dispersed air passes the sharp water-oil interface smoothly

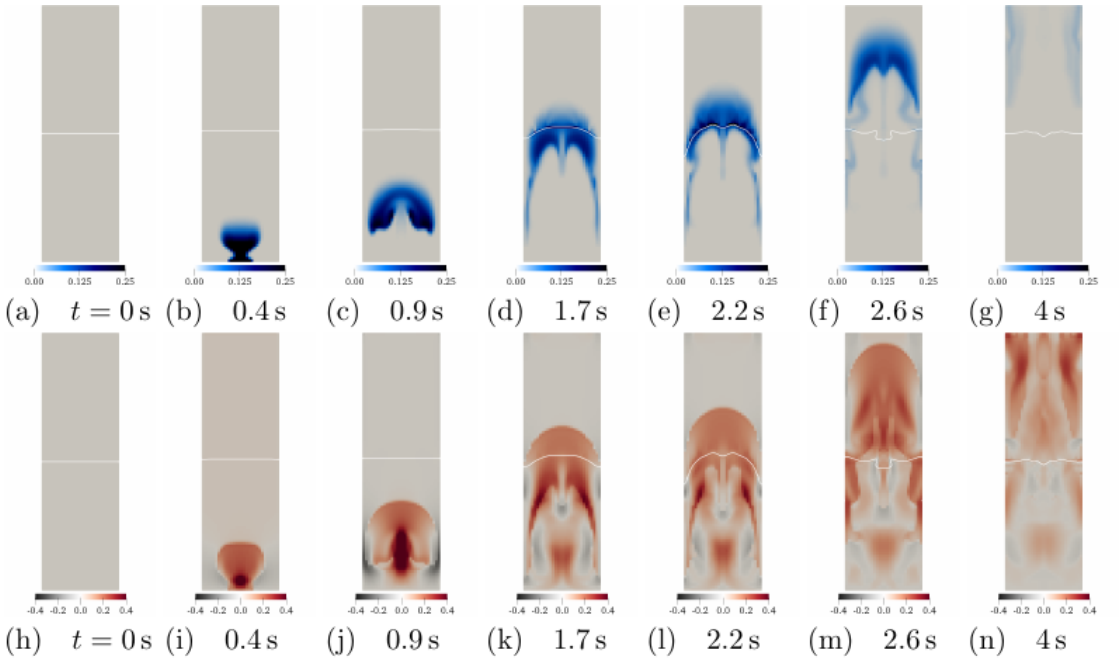

Fig. 5. Top row: contours of volume fraction of dispersed air phase r_α as evolution over time, bottom row: contours of vertical component of velocity fields of dispersed air phase $U_{\mathrm{air},y}$ in ms^{-1} as evolution over time; white lines mark the resolved interface ($r_{\mathrm{water}} = 0.5$) between continuous water and oil phases.

without any oscillatory of the phase velocity field. Note that the phase velocities of water and oil are identical everywhere in the domain. This is a desired behavior and a result of the selected interfacial drag formulation of Štrubelj and Tiselj [29] together with a very small value for the relaxation time τ_r in Eq. (3).

III.C. Three-dimensional Stratified Flow with Turbulence Dampening

The two previous test cases are characterized by a vertical flow, i.e. in the opposite direction to gravitational acceleration, induced by bubbles rising in a stagnant liquid. As the framework is intended to be generally applicable, in the following section results of a horizontal flow configuration are presented, which is not only driven by gravity. The computational domain represents the test section part of the WENKA experimental facility [41]. Only a brief summary of the simulation

TABLE II
Material properties of water, oil, and air in case of a two-dimensional stagnant water-oil stratification with air bubbles.

	Unit	Water	Oil	Air
ρ_α	$\mathrm{kg\,m^{-3}}$	997	990	1.185
μ_α	$\mathrm{Pa\,s}$	0.01	0.01	0.000184
$\sigma_{\mathrm{water-oil}}$	$\mathrm{N\,m^{-1}}$	0.0244		–

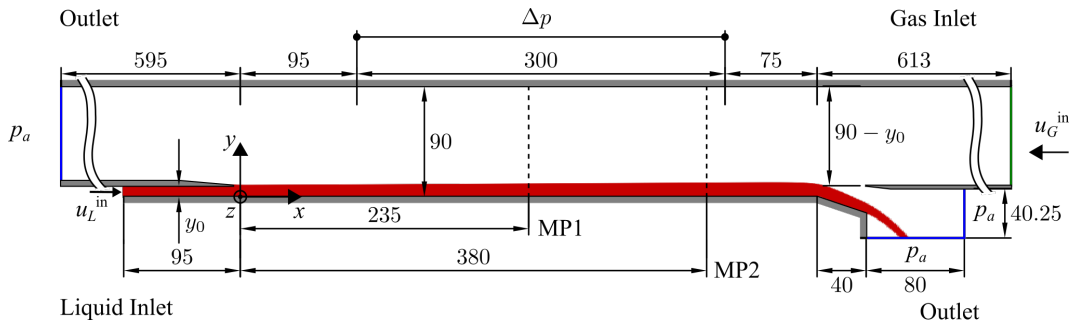

Fig. 6. Computational domain and boundary conditions. The depth of the domain is 110mm. All dimensions are given in mm.

setup and the results is given here. For a detailed introduction and a more elaborated discussion, the reader is referred to Tekavčič et al. [24].

From the WENKA experimental database, the flow conditions 3 and 23 are selected. These cases are characterized by a nearly steady-state supercritical stratified flow. The results are compared for the measurement points MP1 and MP2, where vertical profiles of volume fraction, velocity and turbulence fields were measured. The position as well as the geometry of the simulation domain is shown in Fig. 6. The grid spacings in the channel section of the domain between $0\text{mm} < x < 470\,\text{mm}$ are $\Delta_x = 5\,\text{mm}$, $\Delta_{y,\text{water}} = 1\,\text{mm}$, $\Delta_{y,\text{air}} = 2.6\,\text{mm}$, and $\Delta_z = 5\,\text{mm}$. The total number of grid cells is $N_{\text{cells}} = 176044$. Water enters the channel at the liquid inlet on the bottom left and air enters the gas inlet at the top of the opposite side. Hence, a counter-current flow of water and air develops in the channel section. To ensure physical inlet conditions for a fully developed channel flow and to reduce the computational effort, a field mapping from locations further downstream of the water and air inlets (45 mm for water, 493 mm for air) was used. The boundary conditions are no-slip conditions for water and air at the channel walls and a fixed pressure boundary condition with $p = 100900\,\text{Pa}$ at both outlets. The remaining boundaries are set to homogeneous *Neumann* boundary conditions. An intensive study for various parameters was performed, which includes:

- The evaluation of different turbulence damping approaches: no damping, symmetric damping (both phases) and asymmetric damping (only the gas phase),
- a parametric study on the damping length scale parameter δ_α,
- a mesh sensitivity study using the asymmetric damping approach, and, finally,
- simulations using a three-dimensional domain with symmetric and asymmetric dampening

and a damping parameter of $\delta_\alpha = 7 \cdot 10^{-5}\,\mathrm{m}$.

In the following, we will discuss only results for the three-dimensional domain. The measured and simulated profiles for velocity and turbulent kinetic energy at measurement point MP1 and MP2 are shown in Fig. 7. Independent from the damping strategy, both simulations with the *hybrid model* show good results for velocity as well as turbulent kinetic energy. Compared to other authors, e.g., [33, 16], the quantitative and qualitative agreement of the profiles is similar, which strengthen our confidence in the *hybrid model*. The symmetric turbulence damping tends towards an under-prediction of the turbulent kinetic energy on the liquid side of the interface. The asymmetric damping improves the situation, but this comes at the price of a worse prediction of the streamwise velocity and turbulent kinetic energy at the gas side of the interface. For such relatively smooth interfaces, the *hybrid model* together with the no-slip condition (enforced by the drag model according to Štrubelj and Tiselj [29]) and a turbulence damping works as expected. Nevertheless, for more complex stratified flows, e.g. with unresolved surface waves and droplet entrainment, further modeling is required. In particular, the drag model needs some improvement and should allow some velocity slip, and the hybrid approach should be enabled to handle dispersed phase entrainment and detrainment processes to simulate wave breaking phenomena.

IV. OUTLOOK AND UPCOMING CHALLENGES

The presented *hybrid model* shows good performance for the edge case of sufficiently resolved interfaces as well as for cases where dispersed interfaces interact with resolved ones. The *hybrid model* is implemented into the Euler-Euler framework in OpenFOAM and is available open source [34].

No dedicated validation of the hybrid model for dispersed bubbly flows is carried out as this modeling aspect is captured by relying on the established HZDR baseline model [27, 28]. The upcoming research might focus on the transition between the Euler-Euler and the VOF method as sketched in Fig. 8. In the following, some ideas how to overcome the problems in this transition region and how to enable morphology transitions between the numerical phases will be presented. However, all ideas are speculative and subject to scientific discussions in future.

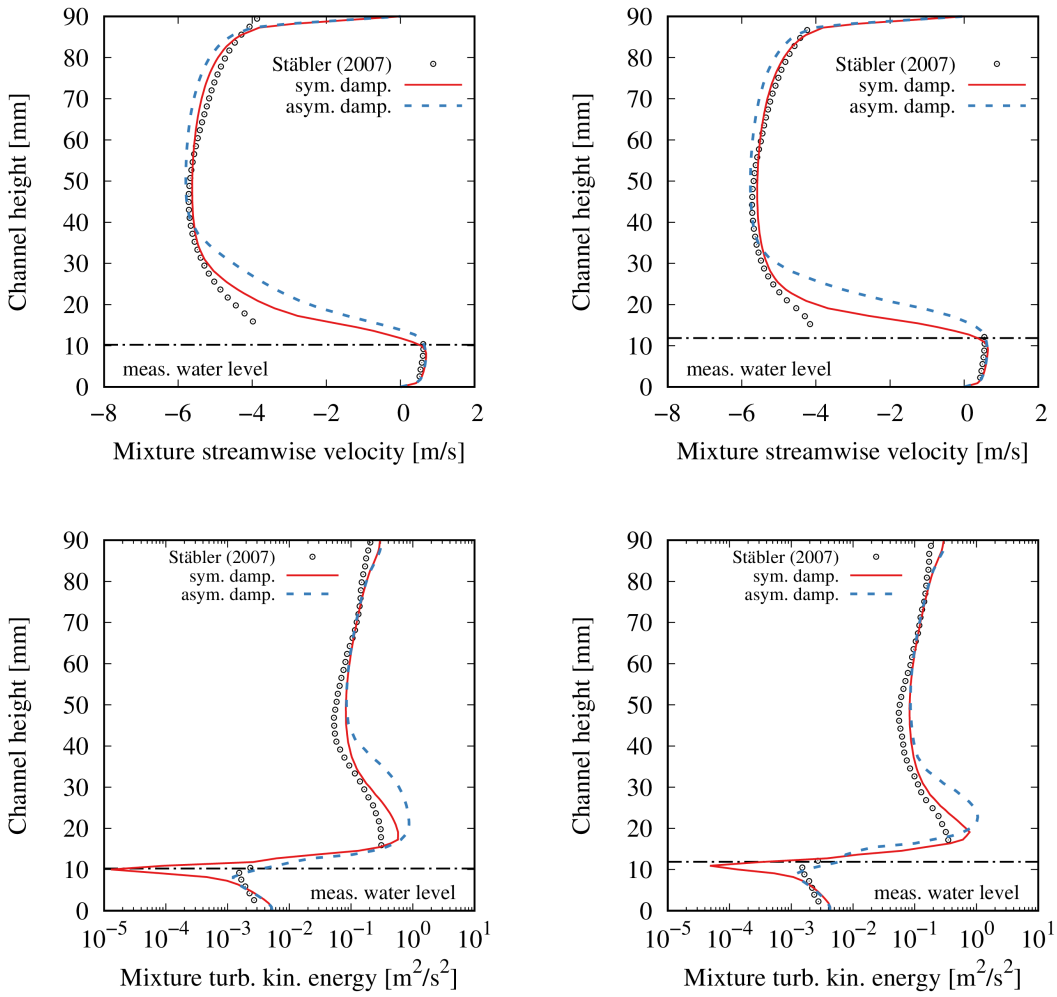

(a) MP1 (b) MP2

Fig. 7. Results for a 3D domain compared to the measured vertical profiles by Stäbler [41]. The horizontal dash-dot line indicates the water level measured in the experiment.

IV.A. Under-resolved Volume-of-fluid Simulations

One of the major problems of algebraic VOF methods is that the mesh resolution has to be sufficiently fine for a good prediction of, e.g. the bubble rising velocity and the bubble shape. However, for a *hybrid model* one needs to extend the validity range of VOF towards coarser mesh resolutions. A coarser mesh resolution results in an artificially enlarged boundary layer of the interface region. This results in a bubble rising velocity, which is much too slow [42]. This effect is clearly visible in Fig. 1, which shows the results of the mesh study for the three-dimensional rising bubble of Balcázar et al. [38]. The interface for $\widetilde{t} = 12.53$ on the coarsest mesh with $\Delta_{\widetilde{x}} = 1/8$ is clearly lagging behind. Contrary to the homogeneous model, the utilized two-fluid

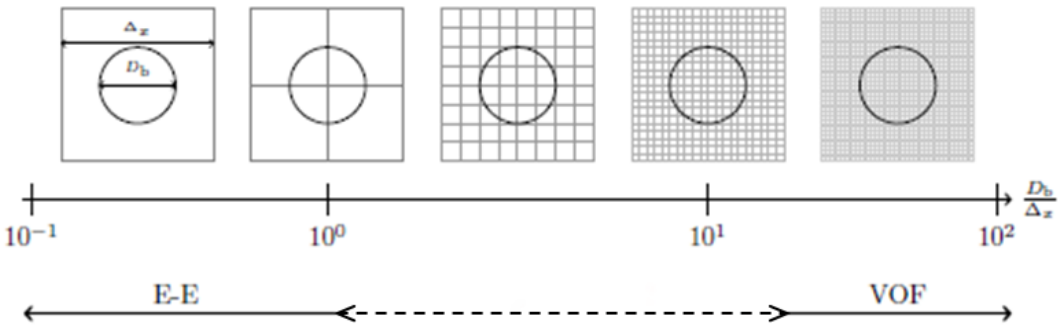

Fig. 8. Bubble diameter versus grid spacing ratio and suitable methods for numerical simulation: Euler-Euler method (E-E) and Volume-of-Fluid method (VOF).

model formulation allows for interfacial slip between the gas and the liquid phase. Hence, the interfacial coupling of Štrubelj and Tiselj [29], which ensures a strong coupling between the phases on a fine grid, has to be blended into a looser coupling on coarser grids. For a fully under-resolved gas bubble, a drag coefficient of $C_D = 0.44$ seems to be reasonable as reported by Gauss et al. [42]. A blending criterion might be the interfacial curvature (inverse of mean radius of a surface) in relation to the grid spacing $\kappa\Delta_x$, which enables blending if curvature is too high to be depicted on the underlying grid. This results in a resolution-adaptive interfacial drag modeling based on the local detection of under-resolved parts of the interface.

IV.B. Over-resolved Euler-Euler simulations

A similar issue exists for the Euler-Euler modeling. Here the validity of the approach has to be extended towards very fine grids. The naive application of the Euler-Euler model on fine grids may lead to convergence problems or unphysical results, something that can be attributed to the inconsistency of the development of the closure models and their application [43]. An example of such a problematic case, a pipe flow with annular gas injection, is shown in Fig. 9, where the void fraction profile shows an unphysical peak in the center of the domain. A simple approach to mimic "coarser meshes" for the closure models is to apply some diffusion to the phase fraction field. This can be understood as a filtering operation. Fig. 9 also shows the results of a proof-of-concept with a suitable diffusion coefficient, which helps to retain a physical void fraction field. However, the amount of diffusion is not known a priori and future activities have to answer the question whether a general rule for the choice of the artificial diffusion can be found.

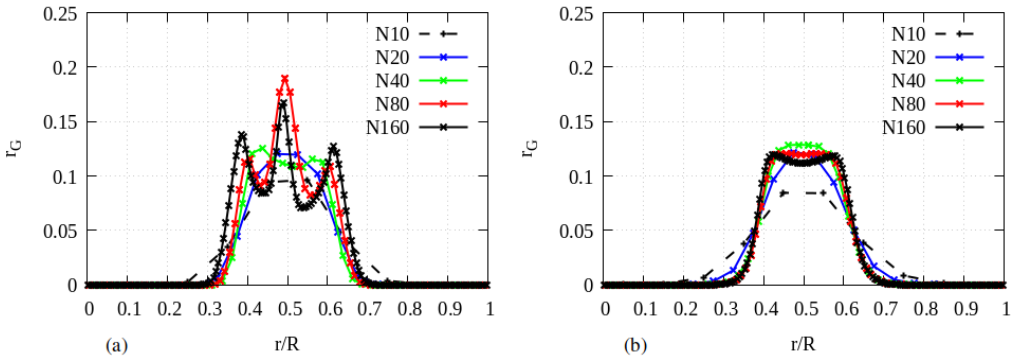

Fig. 9. Gas volume fraction profile in a pipe flow produced by injecting large bubbles with a diameter of $0.2R$ for several refinement levels. The refinement levels correspond to 2 $(4, 8, 16, 32)$ cells per bubble diameter. The Euler-Euler model without diffusion may produce strange results (a), which can be improved by artificial diffusion (b).

IV.C. Transition towards resolved interfaces

Another important mechanism that takes place in the transition region is the morphology transfer between dispersed and continuous phases. This means that small, dispersed bubbles coalesce until they reach a size that is sufficiently large to be resolved on the underlying grid. Furthermore, gas bubbles may enter a different region of the simulation domain that has a grid, which is sufficiently fine to resolve them. Hence, as soon as the grid resolution allows resolving the interface a phase transfer has to be initiated that shifts dispersed phase fraction towards continuous phase fraction. A first step in this direction is a simple threshold model. The phase transfer is active as long as the following condition holds:

$$r_{G,\text{disperse}} + r_{G,\text{continuous}} \geq r_{\text{threshold}}. \tag{8}$$

For a very simple proof-of-concept case presented in Fig. 10, a threshold value of 74% is applied, motivated by the densest packing of spheres. Within a simple rotating flow, it is expected that the gas accumulates in the center region and due to that forms a continuous gas core. Figure 10 illustrates the behavior of the phase transfer model. First, the grid has to be fine enough to enable the transition process. On a coarse grid, the gas just accumulates in a broader region in the center of the domain, but remains dispersed. However, if the mesh is fine enough, the swirl drives the gas towards the center of the domain where the phase transfer takes place and a continuous gas core with a sharp, resolved interface develops. This serves as a conceptual starting point for phase

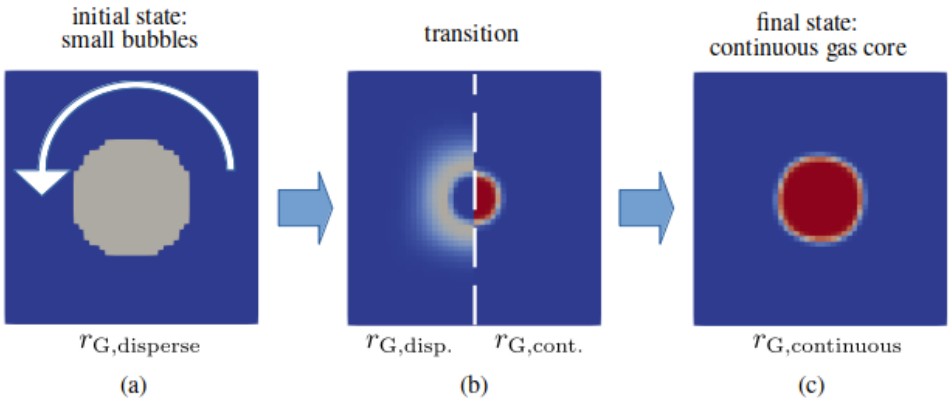

Fig. 10. Disperse bubbles (a) exposed to a rotating liquid are moving to the center of the domain. If the gas phase fraction exceeds the threshold, a transfer from disperse to continuous gas applies (b). Finally, a stable continuous gas core forms (c). Blue indicates a gas phase fraction value of zero, red indicates one.

transfer towards resolved phases and future work has to assess the potential of this simple ansatz.

FUNDING

This work was supported by the Helmholtz European Partnering Program in the project Crossing borders and scales (Crossing). The author from the Jožef Stefan Institute gratefully acknowledges also the financial support provided by the Slovenian Research Agency through the grant P2-0026.

DISCLOSURE

The authors report there are no competing interests to declare.

REFERENCES

[1] D. Lucas, D. Bestion, E. Bodèle, P. Coste, M. Scheuerer, F. D'Auria, D. Mazzini, B. Smith, I. Tiselj, A. Martin et al., "An overview of the pressurized thermal shock issue in the context of the NURESIM project," *Sci. Technol. Nucl. Install.*, **2009** (2008).

[2] M. Herrmann, "A parallel Eulerian interface tracking/Lagrangian point particle multi-scale coupling procedure," *J. Comput. Phys.*, **229**, *3*, 745 (2010); 10.1016/j.jcp.2009.10.009.

[3] J. Ma, C.-T. Hsiao, and G. L. Chahine, "A physics based multiscale modeling of cavitating flows," *Comput. Fluids*, **145**, 68 (2017); 10.1016/j.compfluid.2016.12.010.

[4] J. Hua, "CFD simulations of the effects of small dispersed bubbles on the rising of a single large bubble in 2D vertical channels," *Chem. Eng. Sci.*, **123**, 99 (2015); 10.1016/j.ces.2014.10.035.

[5] A. Boualouache, F. Zidouni Kendil, and A. Mataoui, "Numerical assessment of two phase flow modeling using plunging jet configurations," *Chem. Eng. Res. Des.*, **128**, 248 (2017); 10.1016/j.cherd.2017.10.024.

[6] K. Yan and D. Che, "A coupled model for simulation of the gas-liquid two-phase flow with complex flow patterns," *Int. J Multiph. Flow*, **36**, *4*, 333 (2010); 10.1016/j.ijmultiphaseflow.2009.11.007.

[7] G. Černe, P. Stojan, and I. Tiselj, "Upgrade of the VOF Method for the Simulation of the Dispersed Flow," *Proceedings of ASME FEDSM'00*, ASME 2000 Fluids Engineering Division Summer Meeting (2000).

[8] P. Lopes, J. Leandro, and R. F. Carvalho, "Self-Aeration Modelling Using a Sub-Grid Volume-Of-Fluid Model," *Int. J. Nonlinear Sci. Numer. Simul.*, **18**, *7-8* (2017); 10.1515/ijnsns-2017-0015.

[9] M. Hundshagen, M. Mansour, D. Thévenin, and R. Skoda, "Numerical investigation of two-phase air-water flow in a centrifugal pump with closed or semi-open impeller," *13 th European Conference on Turbomachinery Fluid dynamics & Thermodynamics*, European Turbomachinery Society (2019); 10.29008/ETC2019-011.

[10] M. Hundshagen, M. Mansour, D. Thévenin, and R. Skoda, "3D simulation of gas-laden liquid flows in centrifugal pumps and the assessment of two-fluid CFD methods," *Exp. Comput. Multiph. Flow*, **3**, *3*, 186 (2021); 10.1007/s42757-020-0080-4.

[11] A. De Santis, M. Colombo, B. C. Hanson, and M. Fairweather, "A generalized multiphase modelling approach for multiscale flows," *J. Comput. Phys.*, **436**, 110321 (2021); 10.1016/j.jcp.2021.110321.

[12] M. Colombo, A. De Santis, B. C. Hanson, and M. Fairweather, "Prediction of Horizontal Gas–Liquid Segregated Flow Regimes with an All Flow Regime Multifluid Model," *Processes*, **10**, *5*, 920 (2022); 10.3390/pr10050920.

[13] P. Coste, J. Laviéville, J. Pouvreau, C. Baudry, M. Guingo, and A. Douce, "Validation of the Large Interface Method of NEPTUNE_CFD 1.0.8 for Pressurized Thermal Shock (PTS) applications," *Nucl. Eng. Des.*, **253**, 296 (2012); 10.1016/j.nucengdes.2011.08.066.

[14] P. Porombka and T. Höhne, "Drag and turbulence modelling for free surface flows within the two-fluid Euler-Euler framework," *Chem. Eng. Sci.*, **134**, 348 (2015); 10.1016/j.ces.2015.05.029.

[15] R. V. P. Rezende, R. A. Almeida, A. A. U. de Souza, and S. M. G. U. Souza, "A two-fluid model with a tensor closure model approach for free surface flow simulations," *Chem. Eng. Sci.*, **122**, 596 (2015); 10.1016/j.ces.2014.07.064.

[16] T. Höhne and P. Porombka, "Modelling horizontal two-phase flows using generalized models," *Ann. Nucl. Energy*, **111**, 311 (2018); 10.1016/j.anucene.2017.09.018.

[17] K. Wardle and H. Weller, "Hybrid Multiphase CFD Solver for Coupled Dispersed/Segregated Flows in Liquid-Liquid Extraction," *Int. J. Chem. Eng.*, **2013**, 128936 (2013); 10.1155/2013/128936.

[18] O. Y. Shonibare and K. E. Wardle, "Numerical investigation of vertical plunging jet using a hybrid multifluid-VOF multiphase CFD solver," *Int. J. Chem. Eng.*, **2015**, 1 (2015); 10.1155/2015/925639.

[19] A. Mathur, D. Dovizio, E. M. A. Frederix, and E. M. J. Komen, "A Hybrid Dispersed-Large Interface Solver for multi-scale two-phase flow modelling," *Nucl. Eng. Des.*, **344**, 69 (2019); 10.1016/j.nucengdes.2019.01.020.

[20] H. G. Weller, "A New Approach to VOF-based Interface Capturing Methods for Incompressible and Compressible Flow," , OpenCFD Ltd. (2008).

[21] S. Hänsch, D. Lucas, E. Krepper, and T. Höhne, "A multi-field two-fluid concept for transitions between different scales of interfacial structures," *Int. J. Multiph. Flow*, **47**, 171 (2012); 10.1016/j.ijmultiphaseflow.2012.07.007.

[22] E. M. A. Frederix, D. Dovizio, A. Mathur, and E. M. J. Komen, "All-regime two-phase flow modeling using a novel four-field large interface simulation approach," *Int. J. Multiph. Flow*, **145**, 103822 (2021); 10.1016/j.ijmultiphaseflow.2021.103822.

[23] R. Meller, F. Schlegel, and D. Lucas, "Basic Verification of a Numerical Framework Applied to a Morphology Adaptive Multi-field Two-fluid Model Considering Bubble Motions," *Int. J. Numer. Meth. Fluids*, **93**, *3*, 748 (2021); 10.1002/fld.4907.

[24] M. Tekavčič, R. Meller, and F. Schlegel, "Validation of a morphology adaptive multi-field two-fluid model considering counter-current stratified flow with interfacial turbulence damping," *Nucl. Eng. Des.*, **379**, 111223 (2021); 10.1016/j.nucengdes.2021.111223.

[25] R. Lehnigk, W. Bainbridge, Y. Liao, D. Lucas, T. Niemi, J. Peltola, and F. Schlegel, "An open-source population balance modeling framework for the simulation of polydisperse multiphase flows," *AIChE Journal*, **68**, *3* (2021); 10.1002/aic.17539.

[26] R. Rzehak and E. Krepper, "Bubbly flows with fixed polydispersity: validation of a baseline closure model," *Nucl. Eng. Des.*, **287**, 108 (2015); 10.1016/j.nucengdes.2015.03.005.

[27] Y. Liao, K. Upadhyay, and F. Schlegel, "Eulerian-Eulerian two-fluid model for laminar bubbly pipe flows: Validation of the baseline model," *Comput. Fluids*, **202**, 104496 (2020); 10.1016/j.compfluid.2020.104496.

[28] S. Hänsch, I. Evdokimov, F. Schlegel, and D. Lucas, "A workflow for the sustainable development of closure models for bubbly flows," *Chem. Eng. Sci.*, **244**, 116807 (2021); 10.1016/j.ces.2021.116807.

[29] L. Štrubelj and I. Tiselj, "Two-fluid model with interface sharpening," *Int. J. Numer. Methods Eng.*, **85**, *5*, 575 (2011); 10.1002/nme.2978.

[30] Y. Egorov, "Validation of CFD codes with PTS-relevant test cases," , EVOL-ECORA-D07, ANSYS, Germany, pp. 102–115 (2004).

[31] M. Fulgosi, D. Lakehal, S. Banerjee, and V. De Angelis, "Direct numerical simulation of turbulence in a sheared air-water flow with a deformable interface," *J. Fluid Mech.*, **482**, 319 (2003); 10.1017/s0022112003004154.

[32] F. R. Menter, M. Kuntz, and R. Langtry, "Ten Years of Industrial Experience with the SST Turbulence Model," *Turbulence, Heat and Mass Transfer*, **4**, 625 (2003).

[33] E. Frederix, A. Mathur, D. Dovizio, B. Geurts, and E. Komen, "Reynolds-averaged modeling of turbulence damping near a large-scale interface in two-phase flow," *Nucl. Eng. Des.*, **333**, 122 (2018); 10.1016/j.nucengdes.2018.04.010.

[34] F. Schlegel, M. Draw, I. Evdokimov, S. Hänsch, H. Khan, R. Lehnigk, R. Meller, G. Petelin, and M. Tekavčič, "HZDR Multiphase Addon for OpenFOAM," Rodare (2021); 10.14278/rodare.896., ver. 1.1.0.

[35] A. Cubero, A. Sánchez-Insa, and N. Fueyo, "A consistent momentum interpolation method for steady and unsteady multiphase flows," *Comput. Chem. Eng.*, **62**, 96 (2014); 10.1016/j.compchemeng.2013.12.002.

[36] H. G. Weller, "Bounded Explicit and Implicit Second-Order Schemes for Scalar Transport," , OpenCFD Ltd. (2006).

[37] B. Van Leer, "Towards the ultimate conservative difference scheme III. Upstream-centered finite-difference schemes for ideal compressible flow," *J. Comput. Phys.*, **23**, *3*, 263 (1977); 10.1016/0021-9991(77)90094-8.

[38] N. Balcázar, O. Lehmkuhl, L. Jofre, and A. Oliva, "Level-set simulations of buoyancy-driven motion of single and multiple bubbles," *Int. J. Heat Fluid Flow*, **56**, 91 (2015); 10.1016/j.ijheatfluidflow.2015.07.004.

[39] M. Ishii and N. Zuber, "Drag Coefficient and Relative Velocity in Bubbly, Droplet or Particulate Flows," *AlChE J.*, **25**, *5*, 843 (1979); 10.1002/aic.690250513.

[40] C. T. Crowe, J. D. Schwarzkopf, M. Sommerfeld, and Y. Tsuji, *Multiphase Flow with Droplets and Particles*, CRC Press, 509 pp (2012).

[41] T. D. Stäbler, "Experimentelle Untersuchung und physikalische Beschreibung der Schichtenströmung in horizontalen Kanälen," PhD Thesis, Universität Stuttgart (2007); 10.5445/IR/200068452.

[42] F. Gauss, D. Lucas, and E. Krepper, "Grid studies for the simulation of resolved structures in an Eulerian two-fluid framework," *Nucl. Eng. Des.*, **305**, 371 (2016); 10.1016/j.nucengdes.2016.06.009.

[43] A. Tomiyama, N. Shimada, and H. Asano, "Application of Number Density Transport Equation for the Recovery of Consistency in Multi-Field Model," *Fluids Engineering Division Summer Meeting*, vol. 36975, 501–508 (2003).